Two General Models for Gradient Operators in Imaging

Artyom Grigoryan and Sos Agaian[*], Department of Electrical and Computer Engineering, The University of Texas at San Antonio, USA, [*]Computer Science Department, College of Staten Island and the Graduate Center, Staten Island, NY, USA

Abstract

In this paper we describe two general parametric, non symmetric 3×3 gradient models. Equations for calculating the coefficients of matrices of gradients are presented. These models for generating gradients in x-direction include the known gradient operators and new operators that can be used in graphics, computer vision, robotics, imaging systems and visual surveillance applications, object enhancement, edge detection and classification. The presented approach can be easier extended for large windows.

Introduction

The human visual system is very sensitive to gradients [1]. An image gradient is a directional change in the intensity in the image. It is one of the essential building blocks in many computer vision surveillance systems, security systems, robotic, image retrieval, and image processing applications (including web image applications) [2]-[10]. Gradient magnitude particularly can be used to compute both edge detection and local multi-directional edge orientation. Image gradients are used to create new images with "visualized edges." We consider an edge as the border between two regions, each of which has approximately a uniform intensity. Moreover, image gradients are very important in many graphics, imaging systems, object enhancement, edge detection and classification [11]-[26]. In addition, image gradients used to compute multi-directional orthogonal gradient object phase. One of key tasks of above applications is to find edges, texture, and contours in images/videos. This is because an edge usually can

(a) show the change in light, shade, color, and texture, which is very important to determine the depth, size, orientation and surface properties of a digital image/video;

(b) help to analyze and measure some basic properties related to the object, such as the area, perimeter, visual words, histogram, and shape, which are used for objects identification;

(c) be invariant to monotonic gray-level transformations;

(d) be used to describe enhancement measures and visibility images, or visibility characteristics of grayscale and color images [27]-[44];

(e) be used for extracting the useful information (structure, feature, and properties of objects) from images.

Additionally, one of the key problems in object and person recognition (including pose position and expression recognition) is in extracting essential and accurate features from images of the object, under various lighting conditions or real-world illumination, which may have a huge impact on object recognition performance. To solve this problem, the researchers use different edge detecting gradient operators, which include several variations of such gradients as the Sobel, Robinson, Prewitt, Laplacian and Laplacian of Gaussian gradients [6]-[10].

It should also be noted that, in many images, the over fall will not be sharp because of blurring. The extraction of features in object/facial image representation is an important task in face recognition systems [45]. In face images, the important features of the size, shape, and face orientation are in points of the lines of eyes, nose, lips, and cheekbones. However, in practice, the commonly used edge detection seldom contains perfect contours and edges. It is natural to develop parametric gradient models that are based on the application and able to a) minimize number of false edges and contours; b) generate only a single mark on each edge; c) suppress the noise in computed gradient images; and d) get good localization of edges, textures, and contours.

In this paper, we describe two general parametric 3×3 Gradients models. These models of generating gradients in the x-direction include the known gradient operators (such as Sobel, Robinson, and Prewitt gradients) and new operators that can be used in imaging. Equations for calculating coefficients of gradient matrices are presented. The case of 3×3 window is considered; the models for windows of larger size can be described in a similar way [43,45]. Examples of application of the gradients are given.

General Model of 3×3 Gradients of the 2nd order

Different gradient operators are used in image processing and edge detection and with different size of windows, such as 3×3, 5×5, 7×7, and even 9×9 for large images. In this section, we introduce two models of generating gradients in x-direction, which include the known gradient operators and new operators. The case of 3×3 window is considered.

Type I: Let **A** be the following matrix:

$$\mathbf{A} = \frac{1}{K}\begin{bmatrix} \lambda a & d & -a \\ \lambda b & 0 & -b \\ \lambda c & e & -c \end{bmatrix}, \qquad (1)$$

where the triplet of nonnegative numbers (a, b, c) and number $\lambda > 0$ are given. The coefficients d and e will be found or selected from the condition that the sum of all coefficients equals zero. The scale factor $1/K$ is calculated after the coefficients d and e. This parameterized matrix **A** is called the $(\lambda, a, b, c|d)$-matrix.

Zeroing the sum of all coefficients, we have the following:

$$(a + b + c)(\lambda - 1) + (d + e) = 0,$$
or,
$$(d + e) = -(a + b + c)(\lambda - 1). \qquad (2)$$

In the simple $e = d$ case, that we call *the symmetric case*,

$$d = -\frac{1}{2}(a + b + c)(\lambda - 1). \qquad (3)$$

For simplicity, it is assumed that $a, b, c > 0$. Then, the values of d and e will be negative if $\lambda > 1$ and positive when $\lambda < 1$.

Example 1: $a = b = c = 1, \lambda = 1$

The $d = e$ case corresponds to the Prewitt gradient operator,

$$d = -\frac{1}{2}(3)(0) = 0, \quad A = \frac{1}{3}\begin{bmatrix} 1 & 0 & -1 \\ 1 & 0 & -1 \\ 1 & 0 & -1 \end{bmatrix}. \qquad (4)$$

In the non-symmetric case, $d + e = 0$, the matrix has the form

$$A = \frac{1}{3 + |d|}\begin{bmatrix} 1 & d & -1 \\ 1 & 0 & -1 \\ 1 & -d & -1 \end{bmatrix}.$$

For instance, when $d = 1, 2$, and 0.5, such matrices are

$$\frac{1}{4}\begin{bmatrix} 1 & 1 & -1 \\ 1 & 0 & -1 \\ 1 & -1 & -1 \end{bmatrix}, \quad \frac{1}{5}\begin{bmatrix} 1 & 2 & -1 \\ 1 & 0 & -1 \\ 1 & -2 & -1 \end{bmatrix}, \quad \text{and} \quad \frac{1}{7}\begin{bmatrix} 2 & 1 & -2 \\ 2 & 0 & -2 \\ 2 & -1 & -2 \end{bmatrix}.$$

Example 2: $a = c = 1, b = 2, \lambda = 1$

The $d = e$ case corresponds to the Sobel gradient operator,

$$d = -\frac{1}{2}(4)(0) = 0, \quad A = \frac{1}{4}\begin{bmatrix} 1 & 0 & -1 \\ 2 & 0 & -2 \\ 1 & 0 & -1 \end{bmatrix}. \qquad (5)$$

In the non symmetric case, $d + e = 0$, i.e., the matrix has the form

$$A = \frac{1}{4 + |d|}\begin{bmatrix} 1 & d & -1 \\ 2 & 0 & -2 \\ 1 & -d & -1 \end{bmatrix}.$$

For instance, when $d = 1, 2$, and 0.5, such matrices are

$$\frac{1}{5}\begin{bmatrix} 1 & 1 & -1 \\ 2 & 0 & -2 \\ 1 & -1 & -1 \end{bmatrix}, \quad \frac{1}{6}\begin{bmatrix} 1 & 2 & -1 \\ 2 & 0 & -2 \\ 1 & -2 & -1 \end{bmatrix}, \quad \frac{1}{9}\begin{bmatrix} 2 & 1 & -2 \\ 4 & 0 & -4 \\ 2 & -1 & -2 \end{bmatrix}. \qquad (6)$$

Example 3: $a = c = 1, b = 2, \lambda = 2$

In the symmetric case,

$$d = -\frac{1}{2}(4)(1) = -2, \quad A = \frac{1}{8}\begin{bmatrix} 2 & -2 & -1 \\ 4 & 0 & -2 \\ 2 & -2 & -1 \end{bmatrix}.$$

In the non-symmetric case, $d + e = -4$ and the matrix has the form

$$A = \frac{1}{8 + d}\begin{bmatrix} 2 & d & -1 \\ 4 & 0 & -2 \\ 2 & -4 - d & -1 \end{bmatrix} \qquad (d > 0).$$

If $d < 0$, the scale factor is $1/8$ or $1/(4 - d)$, depending on $d > -4$ or $d < -4$, respectively.

When $d = 1$ and 2, we obtain the matrices

$$\frac{1}{9}\begin{bmatrix} 2 & 1 & -1 \\ 4 & 0 & -2 \\ 2 & -5 & -1 \end{bmatrix} \quad \text{and} \quad \frac{1}{10}\begin{bmatrix} 2 & 2 & -1 \\ 4 & 0 & -2 \\ 2 & -6 & -1 \end{bmatrix}.$$

Example 4: $a = c = 1, b = \sqrt{2}, \lambda = 1$

In the symmetric case,

$$d = -\frac{1}{2}(2 + \sqrt{2})(0) = 0, \quad A = \frac{1}{2 + \sqrt{2}}\begin{bmatrix} 1 & 0 & -1 \\ \sqrt{2} & 0 & -\sqrt{2} \\ 1 & 0 & -1 \end{bmatrix}. \qquad (7)$$

This matrix is for the Frei-Chen gradient operator.

In the non-symmetric case, $d + e = 0$ and

$$A = \frac{1}{2 + d + \sqrt{2}}\begin{bmatrix} 1 & d & -1 \\ \sqrt{2} & 0 & -\sqrt{2} \\ 1 & -d & -1 \end{bmatrix} \qquad (d > 0).$$

For $d = 1$ and $\sqrt{2}$, we obtain the following matrices:

$$A = \frac{1}{3 + \sqrt{2}}\begin{bmatrix} 1 & 1 & -1 \\ \sqrt{2} & 0 & -\sqrt{2} \\ 1 & -1 & -1 \end{bmatrix}$$

and

$$A = \frac{1}{2(1 + \sqrt{2})}\begin{bmatrix} 1 & \sqrt{2} & -1 \\ \sqrt{2} & 0 & -\sqrt{2} \\ 1 & -\sqrt{2} & -1 \end{bmatrix}.$$

Example 5: $a = c = 1, b = (1 + \sqrt{5})/2, \lambda = 1$

In the symmetric case, we obtain the Gold-Ratio matrix

$$d = 0, \quad A = \frac{2}{5 + \sqrt{5}}\begin{bmatrix} 1 & 0 & -1 \\ \frac{1 + \sqrt{5}}{2} & 0 & -\frac{1 + \sqrt{5}}{2} \\ 1 & 0 & -1 \end{bmatrix}$$

$$= \frac{1}{5 + \sqrt{5}}\begin{bmatrix} 2 & 0 & -2 \\ 1 + \sqrt{5} & 0 & -1 - \sqrt{5} \\ 2 & 0 & -2 \end{bmatrix}.$$

In the non-symmetric case, $d + e = 0$ and

$$A = \frac{1}{5 + 2d + \sqrt{5}}\begin{bmatrix} 2 & 2d & -2 \\ 1 + \sqrt{5} & 0 & -1 - \sqrt{5} \\ 2 & -2d & -2 \end{bmatrix} \qquad (d > 0).$$

If $d = 1$, we obtain the matrix

$$A = \frac{1}{7 + \sqrt{5}}\begin{bmatrix} 2 & 2 & -2 \\ 1 + \sqrt{5} & 0 & -1 - \sqrt{5} \\ 2 & -2 & -2 \end{bmatrix}. \qquad (8)$$

In the $d = (1 + \sqrt{5})/2$ case,

$$A = \frac{1}{2(3 + \sqrt{5})}\begin{bmatrix} 2 & 1 + \sqrt{5} & -2 \\ 1 + \sqrt{5} & 0 & -1 - \sqrt{5} \\ 2 & -1 - \sqrt{5} & -2 \end{bmatrix}.$$

Example 6: $a = b = c = 1, \lambda = 5/3$

In the symmetric case, we obtain the following:

$$d = -\frac{1}{2}(3)\left(\frac{2}{3}\right) = -1, \quad A = \frac{1}{5}\begin{bmatrix} 5/3 & -1 & -1 \\ 5/3 & 0 & -1 \\ 5/3 & -1 & -1 \end{bmatrix}$$

$$= \frac{1}{15}\begin{bmatrix} 5 & -3 & -3 \\ 5 & 0 & -3 \\ 5 & -3 & -3 \end{bmatrix}.$$

This matrix corresponds to the Kirsch gradient operator.

In the non-symmetric case, $d + e = -2$, the matrix A has the form

$$A = \frac{1}{5+d}\begin{bmatrix} 5/3 & d & -1 \\ 5/3 & 0 & -1 \\ 5/3 & -2-d & -1 \end{bmatrix} \qquad (d > 0).$$

For the $d = 1$ case, we obtain the matrix

$$A = \frac{1}{6}\begin{bmatrix} 5/3 & 1 & -1 \\ 5/3 & 0 & -1 \\ 5/3 & -3 & -1 \end{bmatrix} = \frac{1}{18}\begin{bmatrix} 5 & 3 & -3 \\ 5 & 0 & -3 \\ 5 & -9 & -3 \end{bmatrix}. \qquad (9)$$

For the $d = 1/2$ case, we obtain the matrix

$$A = \frac{1}{5+1/2}\begin{bmatrix} 5/3 & 1/2 & -1 \\ 5/3 & 0 & -1 \\ 5/3 & -5/2 & -1 \end{bmatrix} = \frac{1}{33}\begin{bmatrix} 10 & 3 & -6 \\ 10 & 0 & -6 \\ 10 & -15 & -6 \end{bmatrix}.$$

Now, we consider more cases with $d < 1$.
Example 7: $a = c = 1, b = 2, \lambda = 1/2$
In this case, we can consider the calculations

$$e = d = -\frac{1}{2}(4)\left(-\frac{1}{2}\right) = 1,$$

$$A = \frac{1}{4}\begin{bmatrix} 1/2 & 1 & -1 \\ 1 & 0 & -2 \\ 1/2 & 1 & -1 \end{bmatrix} = \frac{1}{8}\begin{bmatrix} 1 & 2 & -2 \\ 2 & 0 & -4 \\ 1 & 2 & -2 \end{bmatrix}.$$

Example 8: $a = b = c = 1, \lambda = 1/2$
In this case, we can consider the following calculations for $d, e > 0$:

$$d + e = -(3)\left(-\frac{1}{2}\right) = 3/2, \quad A = \frac{1}{3}\begin{bmatrix} 1/2 & d & -1 \\ 1/2 & 0 & -1 \\ 1/2 & e & -1 \end{bmatrix}.$$

If $d = 1$ and $e = 1/2$, then

$$A = \frac{1}{3}\begin{bmatrix} 1/2 & 1 & -1 \\ 1/2 & 0 & -1 \\ 1/2 & 1/2 & -1 \end{bmatrix} = \frac{1}{6}\begin{bmatrix} 1 & 2 & -2 \\ 1 & 0 & -2 \\ 1 & 1 & -2 \end{bmatrix}.$$

If $d = e = 3/4$, then

$$A = \frac{1}{3}\begin{bmatrix} 1/2 & 3/4 & -1 \\ 1/2 & 0 & -1 \\ 1/2 & 3/4 & -1 \end{bmatrix} = \frac{1}{12}\begin{bmatrix} 2 & 3 & -4 \\ 2 & 0 & -4 \\ 2 & 3 & -4 \end{bmatrix}.$$

In the above model, or model of type I, it is assumed that the central coefficient is zero. We can remove this constrain and consider a new model that is called the model of type II.

Model of Matrices of Type II
Type II: Let **A** be the following matrix:

$$A = \frac{1}{K}\begin{bmatrix} \lambda a & d & -a \\ \lambda b & f & -b \\ \lambda c & e & -c \end{bmatrix}, \qquad (10)$$

where the triplet $(a, b, c) > 0$ and number $\lambda > 0$ are given. The coefficients d, e and f will be found from the condition that the sum of all coefficients equals zero. The matrix is called the $(\lambda, a, b, c|d, e)$-matrix. The scale factor $1/K$ will be found after the coefficients d, e, and f. Zeroing the the sum of all coefficients, we have the following:

$$(a + b + c)(\lambda - 1) + (d + e + f) = 0. \qquad (11)$$

If we assume that $e = d$, then

$$(2d + f) = -(a + b + c)(\lambda - 1).$$

Next, we consider a few examples for the $e = d$ case.
Example 9: $a = b = c = 1, \lambda = 1$

$$2d + f = -\frac{1}{2}(1)(0) = 0, \quad A = \frac{1}{K}\begin{bmatrix} 1 & d & -1 \\ 1 & f & -1 \\ 1 & d & -1 \end{bmatrix}.$$

If $d = 1$, then $f = -2$ and we obtain the matrix of the Prewitt gradient

$$A = \frac{1}{5}\begin{bmatrix} 1 & 1 & -1 \\ 1 & -2 & -1 \\ 1 & 1 & -1 \end{bmatrix}. \qquad (12)$$

Example 10: $a = c = 0, b = 1, \lambda = 1$

$$2d + f = 0, \quad A = \frac{1}{K}\begin{bmatrix} 0 & d & 0 \\ 1 & f & -1 \\ 0 & d & 0 \end{bmatrix}.$$

If $d = 1$, then $f = -2$ and we obtain the matrix

$$A = \frac{1}{3}\begin{bmatrix} 0 & 1 & 0 \\ 1 & -2 & -1 \\ 0 & 1 & 0 \end{bmatrix}.$$

If $d = 1/2$, then $f = -1$ and we obtain the matrix

$$A = \frac{1}{2}\begin{bmatrix} 0 & 1/2 & 0 \\ 1 & -1 & -1 \\ 0 & 1/2 & 0 \end{bmatrix} = \frac{1}{4}\begin{bmatrix} 0 & 1 & 0 \\ 2 & -2 & -2 \\ 0 & 1 & 0 \end{bmatrix}.$$

If $d = 1/4$, then $f = -1/2$ and the matrix is

$$A = \frac{2}{3}\begin{bmatrix} 0 & 1/4 & 0 \\ 1 & -1/2 & -1 \\ 0 & 1/4 & 0 \end{bmatrix} = \frac{1}{6}\begin{bmatrix} 0 & 1 & 0 \\ 4 & -2 & -4 \\ 0 & 1 & 0 \end{bmatrix}.$$

If $d = 0$, then $f = 0$ and the matrix (the separate 1st order gradient)

$$A = \begin{bmatrix} 0 & 0 & 0 \\ 1 & 0 & -1 \\ 0 & 0 & 0 \end{bmatrix}. \qquad (13)$$

Example 11: $a = c = 1, b = 0, \lambda = 1$

$$2d + f = 0, \quad A = \frac{1}{K}\begin{bmatrix} 1 & d & -1 \\ 0 & -2d & 0 \\ 1 & d & -1 \end{bmatrix}.$$

If $d = 1$, then $f = -2$ and we obtain the matrix

$$A = \frac{1}{4}\begin{bmatrix} 1 & 1 & -1 \\ 0 & -2 & 0 \\ 1 & 1 & -1 \end{bmatrix}.$$

Example 12: $a = c = 1, b = -2, \lambda = 1$

$$2d + f = 0, \quad A = \frac{1}{K}\begin{bmatrix} 1 & d & -1 \\ -2 & -2d & 2 \\ 1 & d & -1 \end{bmatrix}.$$

Here, $K = 4 + |2d|$. If $d = 1$, then $f = -2$, $K = 6$, and we obtain the matrix

$$A = \frac{1}{6}\begin{bmatrix} 1 & 1 & -1 \\ -2 & -2 & 2 \\ 1 & 1 & -1 \end{bmatrix}.$$

If $d = 2$, then $f = -4$, $K = 8$, and we obtain the matrix

$$A = \frac{1}{8}\begin{bmatrix} 1 & 2 & -1 \\ -2 & -4 & 2 \\ 1 & 2 & -1 \end{bmatrix}.$$

Now, we describe a few gradients given above in detail with examples on images. Given $(\lambda, a, b, c|d)$-matrix A of type I, the gradient operator is defined with this matrix in x-direction, i.e., $[G_x^2] = A$. The matrix of this gradient in y-direction is considered to be calculated as $[G_y^2] = -[G_x^2]' = -A'$. Here, A' is the transpose matrix A. The gradient operator with these matrices can be named the $(\lambda, a, b, c|d)$-gradient operator.

The $(1, 1, 1, 1|0)$-gradient

The (1,1,1,1|0)-gradient operator is defined by the matrices

$$[G_x^2] = \frac{1}{3}\begin{bmatrix} 1 & 0 & -1 \\ 1 & 0 & -1 \\ 1 & 0 & -1 \end{bmatrix} \quad \text{and} \quad [G_y^2] = \frac{1}{3}\begin{bmatrix} -1 & -1 & -1 \\ 0 & 0 & 0 \\ 1 & 1 & 1 \end{bmatrix}.$$

These matrices are known as the matrices of the Prewitt 3-level gradient operators. Therefore, we denote $[P_x^2] = [G_x^2]$ and $[P_y^2] = [G_y^2]$. Given image f, the gradient images in x- and y-directions are calculated by $P_x^2(f)$ and $P_y^2(f)$, respectively.

The $(1, 1, 1, 1|1/4)$-gradient

The (1,1,1,1|1/4)-gradient is defined with matrices

$$[G_x^2] = \frac{4}{13}\begin{bmatrix} 1 & 1/4 & -1 \\ 1 & 0 & -1 \\ 1 & -1/4 & -1 \end{bmatrix} = \frac{1}{13}\begin{bmatrix} 4 & 1 & -4 \\ 4 & 0 & -4 \\ 4 & -1 & -4 \end{bmatrix}$$

$$\text{and} \quad [G_y^2] = \frac{1}{13}\begin{bmatrix} -4 & -4 & -4 \\ -1 & 0 & 1 \\ 4 & 4 & 4 \end{bmatrix}.$$

As an example, we consider the 512×512 image shown in Fig. 1. Figure 2 shows the gradient images $G_x^2(f)$ and $G_y^2(f)$ in parts (a) and (b), respectively.

Figure 1. (a) The grayscale (binary) image

The maximum gradient image $G_m(f) = \max\{G_x^2(f), G_y^2(f)\}$ is shown in part (c).

(a) x-gradient   (b) y-gradient   (c) maximum
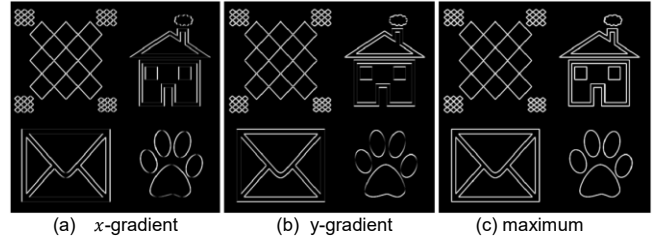
Figure 2. (a) The horizontal, (b) the vertical, and (c) the maximum gradient images.

One can notice the slightly bright horizontal and vertical lines in the gradient images $G_x^2(f)$ and $G_y^2(f)$, respectively, which are due to the nonzero coefficient $d = -e = 1/4$. Indeed, the matrix $[G_x^2]$ can be written as

$$[G_x^2] = \frac{12}{13} \cdot \frac{1}{3}\begin{bmatrix} 1 & 0 & -1 \\ 1 & 0 & -1 \\ 1 & 0 & -1 \end{bmatrix} + \frac{1}{13} \cdot \begin{bmatrix} 0 & 1 & 0 \\ 0 & 0 & 0 \\ 0 & -1 & 0 \end{bmatrix},$$

i.e., this matrix is the arithmetic mean of two matrices, one matrix is the matrix of the Prewitt gradient in the x-direction and another one is matrix of the separated gradient in the y-direction that is given in Eq. 13,

$$[G_x^2] = \frac{12}{13}[P_x^2] + \frac{1}{13}[G_y]. \tag{14}$$

The weight of the separated gradient G_y is 1/13 which is a small number, when comparing with the weight 12/13 of the gradient P_x^2. Therefore, in the gradient image shown in Fig. 2(a), the extracted horizontal lines do not have high intensities. For the gradient G_y^2, similar calculations hold

$$[G_y^2] = -[G_x^2]' = -\frac{12}{13}[P_x^2]' - \frac{1}{13}[G_x]' = \frac{12}{13}[P_y^2] + \frac{1}{13}[G_y],$$

and the intensity of the vertical lines in the gradient image in Fig. 2(b) have low intensity because of the weighted coefficient 1/13. To see better the horizontal and vertical lines in the gradient images $G_x^2(f)$ and $G_y^2(f)$, the value of the coefficient in the $(1,1,1,1|d)$-matrix should be increased.

The (1,1,1,1|1/2)-gradient is defined with matrices

$$[G_x^2] = \frac{2}{7}\begin{bmatrix} 1 & 1/2 & -1 \\ 1 & 0 & -1 \\ 1 & -1/2 & -1 \end{bmatrix} = \frac{1}{7}\begin{bmatrix} 2 & 1 & -2 \\ 2 & 0 & -2 \\ 2 & -1 & -2 \end{bmatrix}$$

and

$$[G_y^2] = \frac{1}{7}\begin{bmatrix} -2 & -2 & -2 \\ -1 & 0 & 1 \\ 2 & 2 & 2 \end{bmatrix}.$$

The matrix $[G_x^2]$ can be written as

$$[G_x^2] = \frac{2}{7}\begin{bmatrix} 1 & 1/2 & -1 \\ 1 & 0 & -1 \\ 1 & -1/2 & -1 \end{bmatrix}$$
$$= \frac{6}{7}\cdot\frac{1}{3}\begin{bmatrix} 1 & 0 & -1 \\ 1 & 0 & -1 \\ 1 & 0 & -1 \end{bmatrix} + \frac{1}{7}\cdot\begin{bmatrix} 0 & 1 & 0 \\ 0 & 0 & 0 \\ 0 & -1 & 0 \end{bmatrix}.$$

Thus, in this arithmetic mean of two matrices

$$[G_x^2] = \frac{6}{7}[P_x^2] + \frac{1}{7}[G_y]. \tag{15}$$

The weight 6/7 of the Prewitt gradient in x-direction is smaller than 12/13, and the weight 1/7 of the separated gradient G_y is larger than the weight 1/13 of these gradients in the (1,1,1,1|1/4)-gradient. Therefore, the additional horizontal and vertical lines in the gradient images $G_x^2(f)$ and $G_y^2(f)$ can be better observed.

Figure 3 shows the gradient images $G_x^2(f)$, $G_y^2(f)$, and the maximum gradient image $G_m(f)$ in parts (a), (b), and (c), respectively.

(a) *x*-gradient (b) *y*-gradient (c) maximum
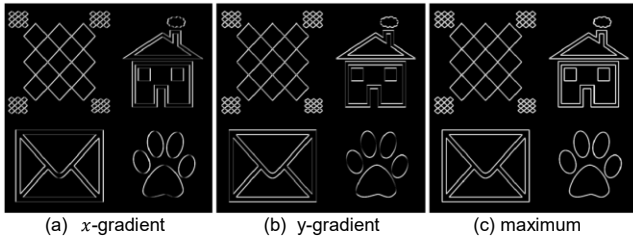
Figure 3. *(a) The horizontal, (b) the vertical, and (c) the maximum gradient images.*

The (1,1,1,1|1)-gradient is defined with matrices

$$[G_x^2] = \frac{1}{4}\begin{bmatrix} 1 & 1 & -1 \\ 1 & 0 & -1 \\ 1 & -1 & -1 \end{bmatrix} \quad\text{and}\quad [G_y^2] = \frac{1}{4}\begin{bmatrix} -1 & -1 & -1 \\ -1 & 0 & 1 \\ 1 & 1 & 1 \end{bmatrix}.$$

Figure 4 shows the gradient images $G_x^2(f)$ and $G_y^2(f)$ in parts (a) and (b), respectively. The maximum gradient image $G_m(f)$ is shown in part (c).

(a) *x*-gradient (b) *y*-gradient (c) maximum
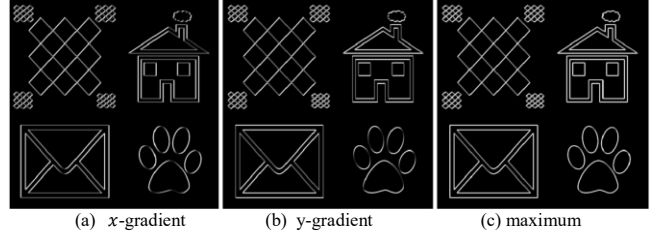
Figure 4. *(a) The horizontal, (b) the vertical, and (c) the maximum gradient images.*

The matrix $[G_x^2]$ can be written as

$$[G_x^2] = \frac{1}{4}\begin{bmatrix} 1 & 1 & -1 \\ 1 & 0 & -1 \\ 1 & -1 & -1 \end{bmatrix} = \frac{3}{4}\cdot\frac{1}{3}\begin{bmatrix} 1 & 0 & -1 \\ 1 & 0 & -1 \\ 1 & 0 & -1 \end{bmatrix} + \frac{1}{4}\cdot\begin{bmatrix} 0 & 1 & 0 \\ 0 & 0 & 0 \\ 0 & -1 & 0 \end{bmatrix}.$$

It is the arithmetic mean of two matrices, i.e., $[G_x^2] = (3/4)[P_x^2] + (1/4)[G_y]$. Thus, when increasing the value of d in the (1,1,1,1|d)-gradient matrix, the weight of the Prewitt gradient is decreasing and the weight of the gradient G_y is increasing. Therefore, the additional horizontal in the gradient image $G_x^2(f)$ becomes more visible.

The $(1, 1, 1.5, 1|d)$-gradient
The gradient is defined by the matrices

$$[G_x^2] = \frac{2}{7+2|d|}\begin{bmatrix} 1 & d & -1 \\ 1.5 & 0 & -1.5 \\ 1 & -d & -1 \end{bmatrix} = \frac{1}{7+2|d|}\begin{bmatrix} 2 & 2d & -2 \\ 3 & 0 & -3 \\ 2 & -2d & -2 \end{bmatrix}$$

and

$$[G_y^2] = \frac{1}{7+2|d|}\begin{bmatrix} -2 & -3 & -2 \\ -2d & 0 & 2d \\ 2 & 3 & 2 \end{bmatrix}.$$

We consider the cases when $d = 0$ and $1/2$, and the matrices $[G_x^2]$ equal

$$\frac{1}{7}\begin{bmatrix} 2 & 0 & -2 \\ 3 & 0 & -3 \\ 2 & 0 & -2 \end{bmatrix} \quad\text{and}\quad \frac{1}{8}\begin{bmatrix} 2 & 1 & -2 \\ 3 & 0 & -3 \\ 2 & -1 & -2 \end{bmatrix}.$$

The second matrix is the arithmetic mean of the first matrix and the matrix of the separated gradient in the y-direction, that is given in Eq. 13,

$$[G_x^2] = \frac{1}{8}\begin{bmatrix} 2 & 1 & -2 \\ 3 & 0 & -3 \\ 2 & -1 & -2 \end{bmatrix} = \frac{7}{8}\cdot\frac{1}{7}\begin{bmatrix} 2 & 0 & -2 \\ 3 & 0 & -3 \\ 2 & 0 & -2 \end{bmatrix} + \frac{1}{8}\cdot\begin{bmatrix} 0 & 1 & 0 \\ 0 & 0 & 0 \\ 0 & -1 & 0 \end{bmatrix}.$$

Therefore, in the gradient image $G_x^2(f)$ with $d = 1/2$, the additional horizontal lines are extracted, when comparing with the $d = 0$ case. In the gradient image $G_y^2(f)$ with $d = 1/2$, the vertical lines are extracted.

Figure 5 shows the gradient images $G_x^2(f)$, $G_y^2(f)$, and the maximum gradient images $G_m(f)$ in parts (a), (b) and (c), respectively, for the cases when $d = 0$ and $d = 1/2$ in the first and second row, respectively.

(a) *x*-gradient   (b) *y*-gradient   (c) maximum
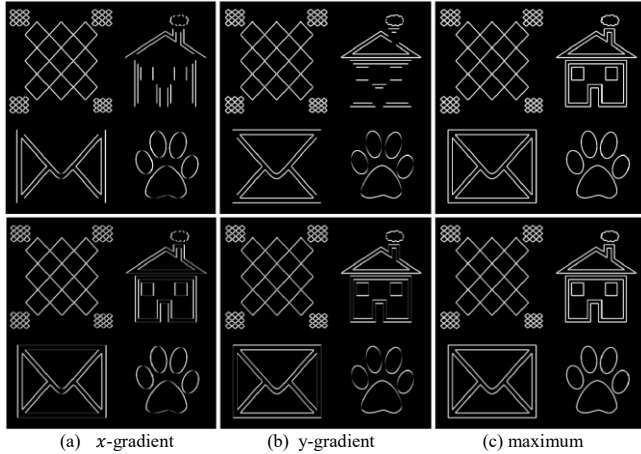
Figure 5. *(a) The horizontal, (b) the vertical, and (c) the maximum gradient images.*

Now, we consider the example with a complex image as the one shown in Fig. 6. The image has been modeled by 20 random rectangles in the square $[0,1] \times [0,1]$ of different intensities which are shown in colors in part (a). Many of these rectangles are overlapped with others. The 256×256 grayscale image calculated as the sum of all these rectangles is shown in part (b).

(a) rectangles   (b) image
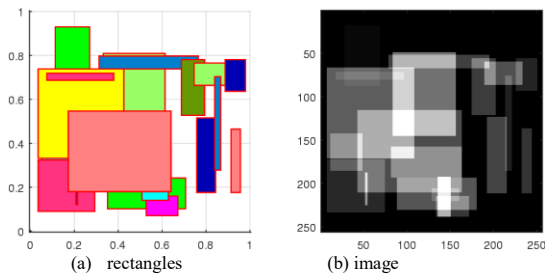
Figure 6. *The grayscale image modeled by 20 random rectangles.*

For this grayscale image, Fig. 7 shows the gradient images $G_x^2(f)$ and $G_y^2(f)$, and the maximum gradient image $G_m(f)$ in parts (a), (b) and (c), respectively.

(a) *x*-gradient   (b) *y*-gradient   (c) maximum
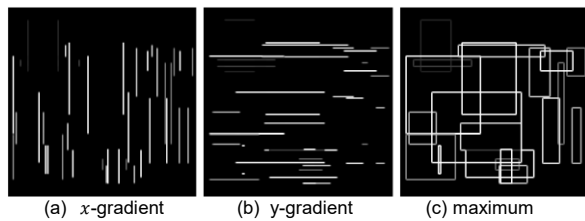
Figure 7. *(a) The horizontal, (b) the vertical, and (c) the maximum gradient images.*

Together with the maximum gradient, the square-root gradient operation is also used for edge detection and it is calculated by the diagram in Fig. 8.
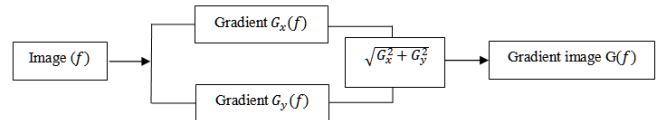
Figure 8. *The diagram of calculation for the square-root gradient image.*

The 3×3 Frei-Chen Gradients

From computation point of view, the Frei-Chen gradient operators can be simplified, by using the coefficients 1.5 instead of coefficients $\sqrt{2} = 1.4142$ in matrices in Eq. 7. The modified matrices are

$$[G_x^2] = \frac{1}{3.5}\begin{bmatrix} 1 & 0 & -1 \\ 1.5 & 0 & -1.5 \\ 1 & 0 & -1 \end{bmatrix} = \frac{1}{7}\begin{bmatrix} 2 & 0 & -2 \\ 3 & 0 & -3 \\ 2 & 0 & -2 \end{bmatrix},$$

$$[G_y^2] = \frac{1}{7}\begin{bmatrix} -2 & -3 & -2 \\ 0 & 0 & 0 \\ 2 & 3 & 2 \end{bmatrix}. \quad (16)$$

These matrices are the $(1,1,1.5,1|0)$-gradient matrices, when $a = 1$, $b = 1.5$, $c = 1$, and $\lambda = 1$. One can also call these matrices the $(1,2,3,2|0)$-matrices.

The matrix of the gradient G_y^2 is defined from G_x^2, by the transposition as $[G_y^2] = -[G_x^2]'$.

The 3×3 Gold-Ratio Gradients

We consider the golden ratio (GR) number $a = \varphi$ instead of $\sqrt{2}$ in Eq. 7, which is the number

$$\varphi = \frac{1 + \sqrt{5}}{2} \approx 1.6180. \quad (17)$$

For the GR, $\varphi^2 = 1 + \varphi$ and $\varphi^3 = 1 + 2\varphi$. The golden ratio is defined as one of the solutions of the equation

$$\varphi = \frac{x + y}{x} = \frac{x}{y}, \quad \text{when } x > y > 0.$$

Figure 9 illustrates the gold ratio. The above equation can also be written as $(x + y)y = x^2$. The illustration of this property as the sum of areas of the rectangle and square is also given in the figure.
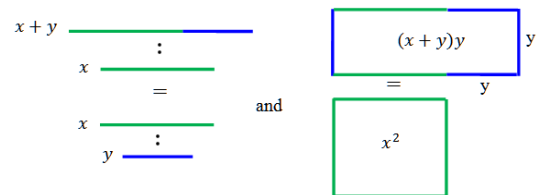
Figure 9. *The illustration of the gold ratio.*

We call the differencing operators in x- and y-directions with matrices

$$[G_x^2] = \frac{1}{2 + \varphi}\begin{bmatrix} 1 & 0 & -1 \\ \varphi & 0 & -\varphi \\ 1 & 0 & -1 \end{bmatrix}, \quad [G_y^2] = \frac{1}{2 + \varphi}\begin{bmatrix} -1 & -\varphi & -1 \\ 0 & 0 & 0 \\ 1 & \varphi & 1 \end{bmatrix}.$$

the Gold-Ratio gradients. The magnitude and square-root Gold-Ratio gradient images is defined as

$$G^2(f) = |G_x^2(f)| + |G_y^2(f)| \text{ and } G(f) = \sqrt{[G_x^2(f)]^2 + [G_y^2(f)]^2}.$$

The Gold-Ratio operators can be generalized by $(1,1,\alpha,1|0)$ −gradient matrices

$$[G_x^2] = \frac{1}{2+|\alpha|}\begin{bmatrix} 1 & 0 & -1 \\ \alpha & 0 & -\alpha \\ 1 & 0 & -1 \end{bmatrix}, \quad [G_y^2] = \frac{1}{2+|\alpha|}\begin{bmatrix} -1 & -\alpha & -1 \\ 0 & 0 & 0 \\ 1 & \alpha & 1 \end{bmatrix}.$$

When $\alpha = 1$, these operators are the Prewitt operators and for $\alpha = 2$, these operators are the Sobel operators. In many cases, the gradient images of these operators look similar; it is visually difficult to distinguish which operator results in the best gradient image after thresholding.

For example, we consider the square-root gradient image

$$G(f) = \sqrt{[G_x^2(f)]^2 + [G_y^2(f)]^2}$$

for the grayscale image shown in Fig. 10.

Figure 10. The grayscale "building" image.

Figure 11 shows the square-root images calculated by the gradient operators for the cases when $\alpha = 1, \varphi$, and 2 in parts (a), (b), and (c), respectively. The images are shown after the thresholding by $T = 20$, i.e., the binary threshold images are calculated at each pixel (n, m) by

$$G_T(f)_{n,m} = \begin{cases} 1, & if \ G(f)_{n,m} \geq T; \\ 0, & if \ G(f)_{n,m} < T. \end{cases} \quad (18)$$

(a) $\alpha = 1$ (b) $\alpha = 1.6180$ (c) $\alpha = 2$
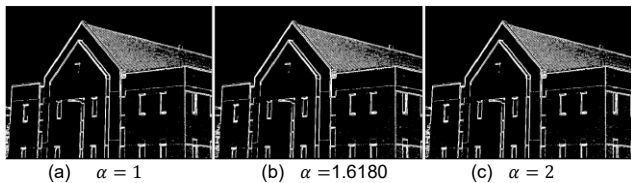
Figure 11. The square-root gradient images after thresholding, when using (a) the Prewitt operator, (b) the Gold-Ratio operator, and (c) the Sobel operator.

Summary

Two models of 3×3 gradient operators have been introduced, which include many known gradients and new gradients that can be used in imaging. Simple equations for calculating the coefficients of the gradient matrices are presented. Such models can also similarly be described for the gradient operators with masks 5×5 and 7×7.

References

[1]   D. Marr, E. Hildrith, "Theory of edge detection," Proc. Royal Society of London, vol. B207, pp. 187-217, 1980.

[2]   W.K. Pratt, Digital Image Processing, 3rd Edition, John Wiley & Sons, Inc., 2001.

[3]   J.M.S. Prewitt, "Object enhancement and extraction,: in Picture Processing and Psychopictorics, Academic Press, New York, 1970.

[4]   R.C. Gonzalez, R.E. Woods, Digital Image Processing, 2nd Edition, Prentice Hall, Upper Saddle River, New Jersey, 2002.

[5]   R.O. Duda, P.E. Hart, Pattern Classification and Scene Analysis, Wiley, New York, 1973.

[6]   G.S. Robinson, "Edge detection by compass gradient masks," Computer Graphics and Image Processing, vol. 6, no. 5, pp. 492-501, 1977.

[7]   G.S. Robinson, "Color edge detection," Proc. SPIE Symposium on Advances in Image Transmission Techniques, vol. 87, San Diego, CA, 1976.

[8]   A. Koschan, M. Abidi, "Detection and classification of edges in color images," IEEE Signal Processing Magazine, vol. 22, no. 1, pp. 64-73, 2005.

[9]   L. Kitchen, A. Rosenfeld, "Edge evaluation using local edge coherence," IEEE Trans. Systems, Man, Cybernetics, vol. SMC-11, no. 9, pp. 597-605, 1981.

[10]   K.A. Panetta, S.S. Agaian, S.C. Nercessian, A.A. Almunstashri, "Shape-dependent canny edge detector," Optical Engineering, vol. 50, no. 8, pp. 087008-087008-12, 2011.

[11]   K.A. Panetta, E.J. Wharton, S.S. Agaian, "Logarithmic edge detection with applications," JCP vol. 3, no. 9, pp. 11-19, JCP, 2008.

[12]   K. Panetta, C. Gao, S. Agaian, S. Nercessian, "A new reference-based edge map quality measure," IEEE Transactions on Systems, Man, and Cybernetics: Systems, vol. 46, no. 11, pp. 1505-1517, 2016.

[13]   C. Gao, K. Panetta, S. Agaian, "New edge detection algorithms using alpha weighted quadratic filter," Proc. IEEE Int. Conf. Syst. Man Cybern., pp. 3167-3172, 2011.

[14]   S.S. Agaian, K.A. Panetta, S.C. Nercessian, E.E. Danahy, "Boolean derivatives with application to edge detection for imaging systems," IEEE Transactions on Systems, Man, and Cybernetics, Part B (Cybernetics) vol. 40, 2010.

[15]   B. Govindarajan, K. Panetta, S. Agaian, "Progressive edge detection on multi-bit images using polynomial-based binarization," Proc. of the ICMLC, pp. 3714-3719, 2008.

[16]   S. Nercessian, K. Panetta, S. Agaian, "A non-reference measure for objective edge map evaluation," Proc. IEEE Int. Conf. Syst. Man Cybernetics, pp. 4563-4568, 2009.

[17]   E. Danahy, S. Agaian, K. Panetta, "Directional edge detection using the logical transform for binary and grayscale images," Proc. SPIE Defense Security Symp.: Mobile Multimedia/Image Process. Military Security Appl., vol. 6250, pp. 625008, 2006.

[18]   E. Danahy, S. Agaian, K. Panetta, "Detecting edges in noisy multimedia environments," Proc. IEEE Int. Symp. Multimedia, pp. 696-700, 2006.

[19] K. Panetta, S. Qazi, S. Agaian, "Techniques for detection and classification of edges in color images," Mobile Multimedia/Image Processing, Security, and Applications, 6982, 69820W, 2008.

[20] B. Govindarajan, K.A. Panetta, S. Agaian, "Image reconstruction for quality assessment of edge detectors," Systems, Man and Cybernetics, SMC 2008. IEEE International Conference, pp. 691-696, 2008.

[21] E.E. Danahy, S.S. Agaian, K.A. Panetta, "Detecting edges in noisy multimedia environments," Multimedia, 2006. ISM'06. Eighth IEEE International Symposium on, pp. 696-700, 2006.

[22] S.C. Nercessian, S.S. Agaian, K.A. Panetta, "A generalized set of kernels for edge and line detection," Proc. SPIE 7245, Image Processing: Algorithms and Systems VII, 72450U, 2009.

[23] S. Nercessian, K. Panetta, S. Agaian, "A parametric method for edge detection based on recursive mean-separate image decomposition," Machine Learning and Cybernetics, International Conference, pp. 3689-3694, 2008.

[24] S. Qazi, K. Panetta, S. Agaian, "Detection and comparison of color edges via median based pca," Systems, Man and Cybernetics, SMC 2008. IEEE International Conference, 2008.

[25] S. Nercessian, K. Panetta, S. Agaian, "Improving edge-based feature extraction using feature fusion," Systems, Man and Cybernetics, SMC 2008. IEEE International Conference, pp. 679-684, 2008.

[26] S. Nercessian, K. Panetta, S. Agaian, "Automatic detection of potential threat objects in x-ray luggage scan images," IEEE. Conf. on Tech. for Home. Security, 2008.

[27] S.S. Agaian, K. Panetta, A.M. Grigoryan, "A new measure of image enhancement," Proc. IASTED Int. Conf. Signal Processing &Communication, Marbella, Spain, 19–22 (2000).

[28] S.S. Agaian, K. Panetta, A.M. Grigoryan, "Transform-based image enhancement algorithms," IEEE Trans. on Image Processing, vol. 10, no. 3, pp. 367–382, 2001.

[29] A.M. Grigoryan, S.S. Agaian, Multidimensional Discrete Unitary Transforms: Representation, Partitioning and Algorithms, Marcel Dekker Inc., New York, 2003.

[30] Z. Rahman, D. Jobson, G.A. Woodell, "Retinex processing for automatic image enhancement," Journal of Electronic Imaging, vol. 13, no. 1, pp. 100-110, 2004.

[31] A.M. Grigoryan and S.S. Agaian, "Adapted Retinex Algorithm with Complexity Optimization for Mobile Phone Medical Image Enhancement," - chapter 5, pp. 119-151. In Electronic Imaging Applications in Mobile Healthcare, J. Tang, S.S. Agaian, and J. Tan, Eds., SPIE Press, Bellingham, Washington, February 2016,

[32] F.T. Arslan, A.M. Grigoryan, "Fast splitting alpha-rooting method of image enhancement: Tensor representation," IEEE Trans. on Image Processing, vol. 15, no. 11, pp. 3375–3384, Nov. 2006.

[33] A.M. Grigoryan, S.S. Agaian, "Monotonic sequences for image enhancement and segmentation," Digital Signal Processing, vol. 41, pp. 70–89, June 2015, (doi:10.1016/j.dsp.2015.02.011)

[34] A.M. Grigoryan, S.S. Agaian, "Preprocessing Tools for Computer-Aided Cancer Imaging Systems," in "Computer-Aided Cancer Detection and Diagnosis: Recent Advances" (Editors: J. Tang and S. Agaian), SPIE, chapter 2, p. 55, 2014.

[35] A.M. Grigoryan, "Two classes of elliptic discrete Fourier transforms: Properties and examples," Journal of Mathematical Imaging and Vision (0235), vol. 39, pp. 210-229, January 2011.

[36] A.M. Grigoryan, S.S. Agaian, "Transform-based image enhancement algorithms with performance measure," Advances in Imaging and Electron Physics, Academic Press, vol. 130, pp. 165–242, 2004.

[37] A.M. Grigoryan, M.M. Grigoryan, Brief Notes in Advanced DSP: Fourier Analysis With MATLAB, CRC Press, Taylor and Francis Group, Boca Raton, New York, 2009.

[38] K.A Panetta, E.J. Wharton, S.S. Agaian, "Human visual system-based image enhancement and logarithmic contrast measure," IEEE Transactions on Systems, Man, and Cybernetics, Part B (Cybernetics), vol. 38, no. 1, pp. 174–188, 2008.

[39] A.M. Grigoryan, J. Jenkinson, S.S. Agaian, "Quaternion Fourier transform based alpha-rooting method for color image measurement and enhancement," SIGPRO-D-14-01083R1, Signal Processing, vol. 109, pp. 269–289, April 2015, (doi:10.1016/j.sigpro.2014.11.019)

[40] A.M. Grigoryan, S.S. Agaian, "Retooling of color imaging in the quaternion algebra," Applied Mathematics and Sciences: An International Journal (MathSJ), vol. 1, no. 3, pp. 23–39, 2014.

[41] A.M. Grigoryan, J. Jenkinson, S.S. Agaian, "Quaternion Fourier transform based alpha-rooting method for color image measurement and enhancement," SIGPRO-D-14-01083R1, Signal Processing, vol. 109, pp. 269–289, 2015.

[42] A.M. Grigoryan, S.S. Agaian, "Color Enhancement and Correction for Camera Cell Phone Medical Images Using Quaternion Tools," Chapter 4, pp. 77–117. In book: Electronic Imaging Applications in Mobile Healthcare, (J. Tang, S.S. Agaian, and J. Tan, Eds.,) SPIE Press, Bellingham, Washington, 2016.

[43] A.M. Grigoryan, S.S. Agaian, Practical Quaternion Imaging With MATLAB, SPIE PRESS, 2018.

[44] A.M. Grigoryan, S.S. Agaian, "Image Processing Contrast Enhancement," p. 22, Wiley Encyclopedia of Electrical and Electronics Engineering, May 2017, (doi: 10.1002/047134608X.W5525.pub2)

[45] A.M. Grigoryan, S.S. Agaian, "Color Facial Image Representation with New Quaternion Gradients," Image Processing: Algorithms and Systems, IS&T Electronic Imaging Symposium, p. 6, 2018.

Author Biography

Artyom Grigoryan received the MS degrees in mathematics from Yerevan State University (1978), in imaging science from Moscow Institute of Physics and Technology (1980), and in electrical engineering from Texas A&M University (1999), and PhD degree in mathematics and physics from Yerevan State University (1990). He is an associate professor of the ECE Department, College of Engineering, University of Texas at San Antonio. He is author of 4 books, 10 book-chapters, 3 patents, 120 papers.

Sos Agaian received the M.S. degree in mathematics and mechanics from Yerevan University, Armenia, the Ph.D. degrees in math and physics from Steklov Institute of Mathematics, Russian Academy of Sciences, and in engineering from Institute of Control System, Russian Academy of Sciences. He is professor of the Science Department, College of Staten Island. He is Fellow of the SPIE, IEEE, AAAS, and IS&T. He has authored of 500 scientific papers, 7 books, holds 14 patents.